Ionic Liquid MOFs Hot Paper

How to cite: *Angew. Chem. Int. Ed.* **2021**, *60*, 1290–1297
International Edition: doi.org/10.1002/anie.202010783
German Edition: doi.org/10.1002/ange.202010783

MOF-Directed Synthesis of Crystalline Ionic Liquids with Enhanced Proton Conduction

Wen-Long Xue[+], Wei-Hua Deng[+], Hui Chen, Rui-Heng Liu, Jared M. Taylor, Yu-kun Li, Lu Wang, Yu-Heng Deng, Wen-Hua Li, Ying-Yi Wen, Guan-E Wang, Chong-Qing Wan, and Gang Xu**

Abstract: *Arranging ionic liquids (ILs) with long-range order can not only enhance their performance in a desired application, but can also help elucidate the vital between structure and properties. However, this is still a challenge and no example has been reported to date. Herein, we report a feasible strategy to achieve a crystalline IL via coordination self-assembly based reticular chemistry.* ***IL$_1$MOF****, was prepared by designing an IL bridging ligand and then connecting them with metal clusters.* ***IL$_1$MOF*** *has a unique structure, where the IL ligands are arranged on a long-range ordered framework but have a labile ionic center. This structure enables* ***IL$_1$MOF*** *to break through the typical limitation where the solid ILs have lower proton conductivity than their counterpart bulk ILs.* ***IL$_1$MOF*** *shows 2–4 orders of magnitude higher proton conductivity than its counterpart IL monomer across a wide temperature range. Moreover, by confining the IL within ultramicropores (< 1 nm),* ***IL$_1$MOF*** *suppresses the liquid–solid phase transition temperatures to lower than −150 °C, allowing it to function with high conductivity in a subzero temperature range.*

Introduction

Changing materials from amorphous to a long-range ordered (crystalline) state is a particularly interesting research realm.[1a,b] Superior to amorphous materials with uncertain structures, crystalline materials enable precise structure determination down to the molecular level via diffraction techniques, which facilitates a deeper fundamental understanding of their structure-property relationships.[1c,d] Moreover, the long-range ordered structure, low defect density, symmetry, and anisotropy of crystalline materials can profoundly enhance their performances, such as better mechanical stability, unique physicochemical properties,[2] and importantly, faster electron/ion transport.[3] One of the biggest challenges in this realm is changing a liquid to a crystal while simultaneously maintaining or enhancing its properties.

Ionic liquids (ILs) are a type of liquid salt that melts near or below room temperature. They have been widely used as safe and promising electrolytes in supercapacitors, secondary batteries, full cells and dye-sensitized solar cells etc.[4] Compared to the classic ILs, the developed solid IL derivatives, including the liquid crystals of semi-rigid poly(ionic liquid)s[5] and the ILs@support systems with ILs confined within nano pore/region of supports (carbon nanotubes, silica, ceramic, (bio)polymer etc.)[6] (Scheme 1), possess significantly enhanced mechanical properties required for practical applications and relative ordered structures in short-range. However, they suffer from significantly lower conductivity than their counterpart bulk ILs[5–7] due to the reduced ion content in the ILs@support systems and absent long-range ordered structure even in liquid-crystal ILs (i.e. Random ILs, Scheme 1). Although solid IL derivatives are proposed as a superior choice for optimizing the manufacture, safety and cost of the various electrical devices, their conductivities generally cannot meet the practical needs ($\approx 10^{-3}$ S cm^{-1}) of applications at room temperature or lower. Moreover, owing to the random states, structure-property-relationship based iterative design to improve their properties is limited. Crystalline ILs combining the high conductivity of liquid-state ILs, high mechanical stability of solid IL, and a long-range ordered structure may greatly favor their application in real-world devices.

Metal-organic frameworks (MOFs) or porous coordination polymers are a type of porous materials with long-range

[*] W. L. Xue[+,++], H. Chen, R. H. Liu, Y. K. Li, L. Wang, Prof. Y. H. Deng, Prof. C. Q. Wan
Beijing Key Laboratory for Optical Materials and Photonic Devices, Department of Chemistry, Capital Normal University
Beijing 100048 (China)
E-mail: wancq@cnu.edu.cn

W. H. Deng[+,++], W. H. Li, Y. Y. Wen, Prof. G. E. Wang, Prof. G. Xu
State Key Laboratory of Structural Chemistry, Fujian Institute of Research on the Structure of Matter, Chinese Academy of Sciences
Fuzhou, Fujian 350002 (China)
E-mail: gxu@fjirsm.ac.cn

W. H. Deng[+,++], Prof. G. Xu
University of Chinese Academy of Sciences, Chinese Academy of Sciences
Beijing 100049 (China)

Prof. G. Xu
Fujian Science & Technology Innovation Laboratory for Optoelectronic Information of China
Fuzhou, Fujian 350108 (China)

Prof. J. M. Taylor
Department of chemistry, University of Calgary
Calgary, Alberta T2N1N4 (Canada)

[+] These authors contributed equally to this work.

[++] Co-first authors.

Supporting information and the ORCID identification number(s) for the author(s) of this article can be found under: https://doi.org/10.1002/anie.202010783.

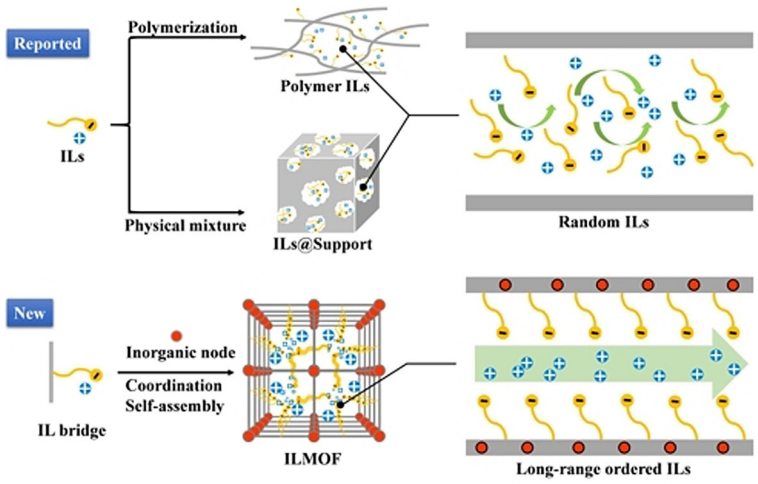

Scheme 1. Strategies for crystalline ILMOF with long-rang ordered framework and traditional solid ILs featuring random structures. Positive and negative signs represent cation and anion in ILs. In the lower panel, the positive signs present H^+ originated from CH_3SO_3H in this work.

ordered structures, which are constructed by coordination bonds between inorganic nodes and organic bridging ligands.[8] Their crystalline structures can be flexibly designed with desired organic ligands to provide versatile properties for applications, such as molecular storage, separation, drug delivery and catalysis.[9] With judiciously designed host-guest interactions, MOFs are promising to transcribe their long-range ordered structure to amorphous molecules/polymers/protein/enzyme, etc. by incorporating them into the micropores.[10] Also inspired by this, ILs were impregnated into MOFs to form ILs@MOF materials by both the H. Kitagawa' group and ours.[11] However, due to the difficulty in precisely controlling the weak interactions (hydrogen bonding, electrostatic interactions, etc.) between ILs and framework of the MOF, the reported ILs@MOF materials failed to show a crystalline IL network in the MOF, with the IL in a random state (Scheme 1). The conductivities of ILs@MOF materials are still far lower than their counterpart bulk ILs.

In this work, we report the preparation of the first example of a IL with long-range ordered structure, **IL_1MOF**, via reticular synthesis strategy to tackle the above-mentioned issues in solid ILs. This was readily realized by designing IL monomers as bridging ligands to connect with metal clusters through a coordination self-assembly based reticular chemistry (Scheme 1).[9h–j] X-ray diffraction, NMR, TGA and DSC measurements determined that **IL_1MOF** is isostructural to that of UiO-67[12] (Figure 1, Scheme S1,S2). Variable-temperature impedance spectroscopy measurements revealed not only an unexpectedly higher proton conductivity of **IL_1MOF** than that of the counterpart bulk **IL_1**, but also a working temperature of **IL_1MOF** down to −40 °C. Cycling variable temperature conductivity tests demonstrated its excellent long-term stability and repeatability. Variable-temperature solid-state nuclear magnetic resonance (SSNMR) measurements were conducted to study the dominant proton dynamics. A possible relationship between the high proton conductivity and crystalline structure of **IL_1MOF** is also discussed.

Results and Discussion

Liquid-state **IL_1**, an ionic liquid bridging ligand for constructing **IL_1MOF**, was prepared by covalently bonding the composite part ([-MIMS][MSA]) of **IL_2** to 4,4′-biphenyldicarboxylate acid (H_2BPDC) (Figure 1a and S1, Scheme S1,S2). **IL_2** bears the composite of 1-(1-ethyl-3-imidazolio)-propane-3-sulfonate (EIMS) and methanesulfonic acid (MSA). The zwitterions (EIMS) combine the MSA to compose a binary ionic liquid with the negative charge shifting between the -SO_3^- on EIMS (or -MIMS) and MSA via H^+ hopping, furnishing a Brønsted acid-base buffer (Figure 1a). Herein, Zr^{IV} based UiO-67 (a MOF with H_2BPDC linker) is chosen as the structure model for **IL_1MOF** due to its high thermal stability and stability to acids. Its two pore types (tetrahedron with $\varphi \approx 12$ Å and octahedron with $\varphi \approx 16$ Å, $V = 3082$ Å^3) are interconnected/shared by triangular windows of $\varphi \approx 8$ Å (Figure 1b and S2)[12] and are large enough to accommodate segment -MIMS (≈ 6.70 Å across). The MOF is synthesized by reaction of H_2BPDC-MIMS with $ZrCl_4$ salt under solvothermal conditions. $Zr_6O_4(OH)_4$(BPDC-MIMS)$_{5.3}$·$(O_2CCH_3)_{1.4}$ (**MIMS-MOF**) was obtained as white powder with 71.2% yield as determined by ^{1}H-NMR spectrum, TGA, ICP and EDX analyses (Figure 1e, S4,S5, and Table S2). Stability tests show **MIMS-MOF** remains intact under high pressure and through a wide pH range (1–10, Figure S6a), which allows for the impregnation of MSA. As shown in Figure 1b and Scheme S2, a volume of MSA (≈ 2 Å across, $V_{vdW} = 70.74$ Å^3)[13] equaling to the total pore volume of **MIMS-MOF** (0.426 cm^3 g^{-1}, Table S3,S4) was incorporated through an incipient wetness technique upon grinding and heating[11,14a,15] (synthesis section in ESI), giving **IL_1MOF**. Wherein the framework, the sulfonic -SO_3^- of the grafted MIMS groups on **MIMS-MOF** can dissociate the MSA through a Brønsted acid-base buffer[14] as that in bulk **IL_1** and **IL_2** (Figure 1a), thus constructing a new type of ionic liquid bearing rigid lattice framework. We term it as crystalline IL (**IL_1MOF**) with a long-range ordered structure of MOF's framework sharp contrast to that random ILs

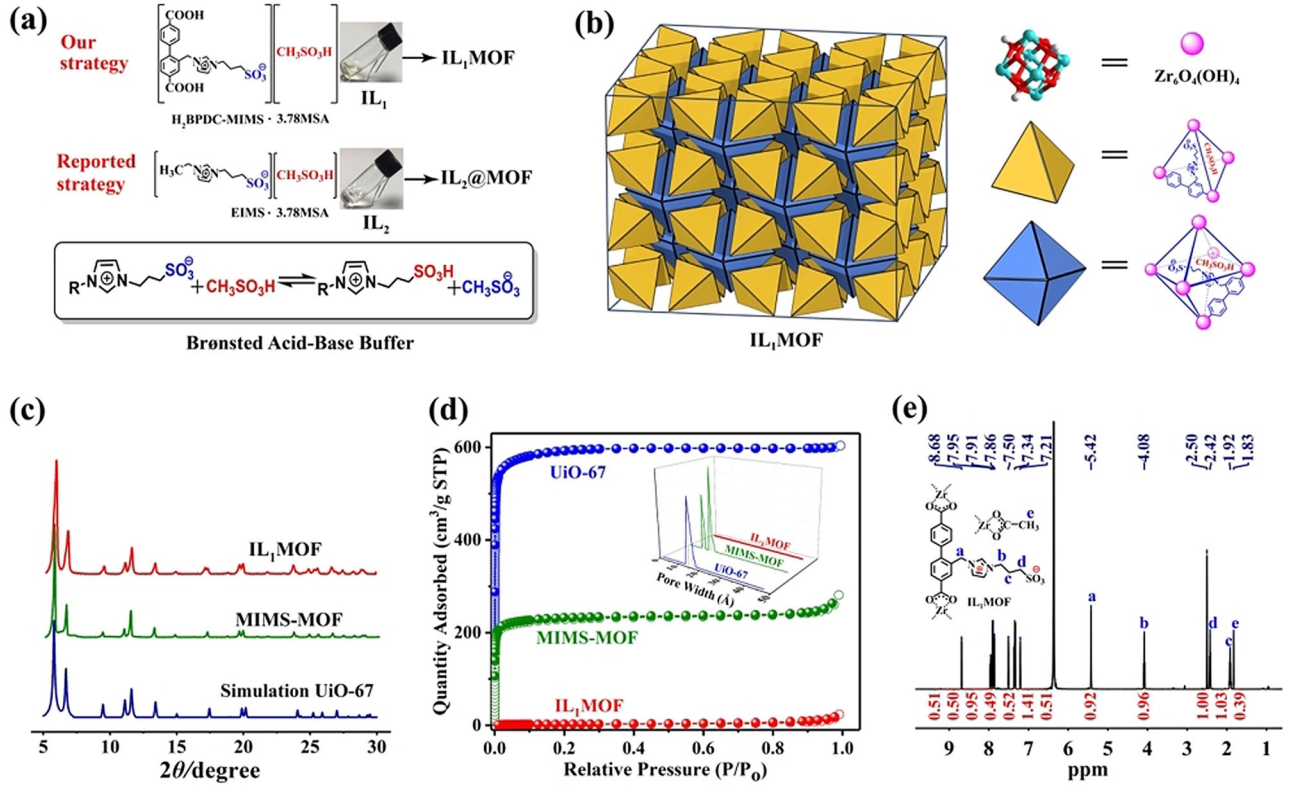

Figure 1. a) Illustrations of **IL_1**, **IL_1MOF**, **IL_2**, **IL_2@MOF** composites. b) Rationalized structure of **IL_1MOF** featuring tetrahedron and octahedron cages constructed with the H_2BPDC-MIMS linkers and $Zr_6O_2(OH)_4$ nodes. c) PXRD patterns, d) N_2 adsorption isotherms and pore-size distributions of **MIMS-MOF**, **IL_1MOF** and UiO-67. e) ^{1}H NMR spectra of activated **MIMS-MOF** digested in deuterium chloride (30 ul) and [D_6]DMSO (500 ul). Deuterium chloride: 6.33 ppm.

reported (Scheme 1). Owing to the already present -MIMS, the incorporated MSA pairs to the zwitterion in more ordered array and the H^+ migration will take place between the sulfonic sites of zwitterions and MSA for fast ion transport along the infinite ultramicropore channels (< 1 nm, subtracted the -MIMS across) (Scheme 1, Figure S2[13]). Based on the formula of **MIMS-MOF** and the incorporated MSA (w% = 38.5%) (Table S4, Figure S4), the stoichiometric formula for **IL_1MOF** is $Zr_6O_4(OH)_4(BPDC\text{-}MIMS)_{5.3}\cdot(O_2CCH_3)_{1.4}\cdot(MSA)_{20.0}$. **$IL_1$MOF** has a [BPDC-MIMS]/[MSA] molar ratio of 1: 3.78, which is same to that of **IL_1**. This composite nature is further evidenced by vide infra solid-state ^{13}C NMR spectra, FT-IR and TGA spectra measurements (Figure S4 and S7). As a reference, UiO-67, $Zr_6O_4(OH)_4(BPDC)_{5.3}\text{-}(O_2CCH_3)_{1.4}$ (determined via ^{1}H-NMR spectrum and TGA, Figure S3 and S4), was also synthesized through the similar procedure, and impregnated with **IL_2** equaling total pore volume of UiO-67 to generate **IL_2@MOF** (Scheme S2, Table S4).

The powder X-ray diffraction (PXRD) fingerprint pattern of **MIMS-MOF** and **IL_1MOF** overlap that of UiO-67[12] (Figure 1c), indicating the similar crystalline framework of these three MOFs. So, as shown in Figure 1b and S2, the $Zr_6O_4(OH)_4$ octahedral clusters connect to adjacent clusters through the **IL_1** bridging linkers and form the tetrahedral and octahedral cages. The tetrahedral cages share triangular windows with the octahedral pores, with each tetrahedral cage surrounded by 4 symmetric octahedrons and each octahedral pore surrounded by 8 symmetric tetrahedrons. Such interconnection of octahedral and tetrahedral cages within the lattice structure form the 3D crystalline pore network and lead to the long-range ordered arrangement of **IL_1** ligands.

Besides PXRD measurements, successful preparations of **MIMS-MOF** and **IL_1MOF** were also confirmed by N_2 absorption experiments. The Brunauer-Emmett-Teller (BET) surface areas change from 2407.42 m^2g^{-1} for UiO-67, to 323.67 m^2g^{-1} for **MIMS-MOF**, and then to the negligible for **IL_1MOF** (Figure 1d, S8 and Table S3), indicating the -MIMS groups protruding to the pore of **MIMS-MOF** and the [-MIMS][MSA] moieties encoded within **IL_1MOF** fill the inner micropore volume of the MOF. Combining these results with the similar morphologies of **MIMS-MOF** and **IL_1MOF** in their scanning electron microscopy (SEM) images (Figure S9), we speculate that MSA molecules do not aggregate on the outer surface of **IL_1MOF** particles, but pair with the BPDC-MIMS to form the **IL_1** within the lattice structure. Thus, the [-MIMS][MSA] moieties are arranged along the ultramicropores channel (< 1 nm).

Temperature-dependent conductivities were measured in an oven through alternating current (AC) impedance spectroscopy analysis with a quasi-four-probe method from −40 to 80 °C. All samples were prepared in dry box under N_2 protection to exclude the possible moisture from the air,

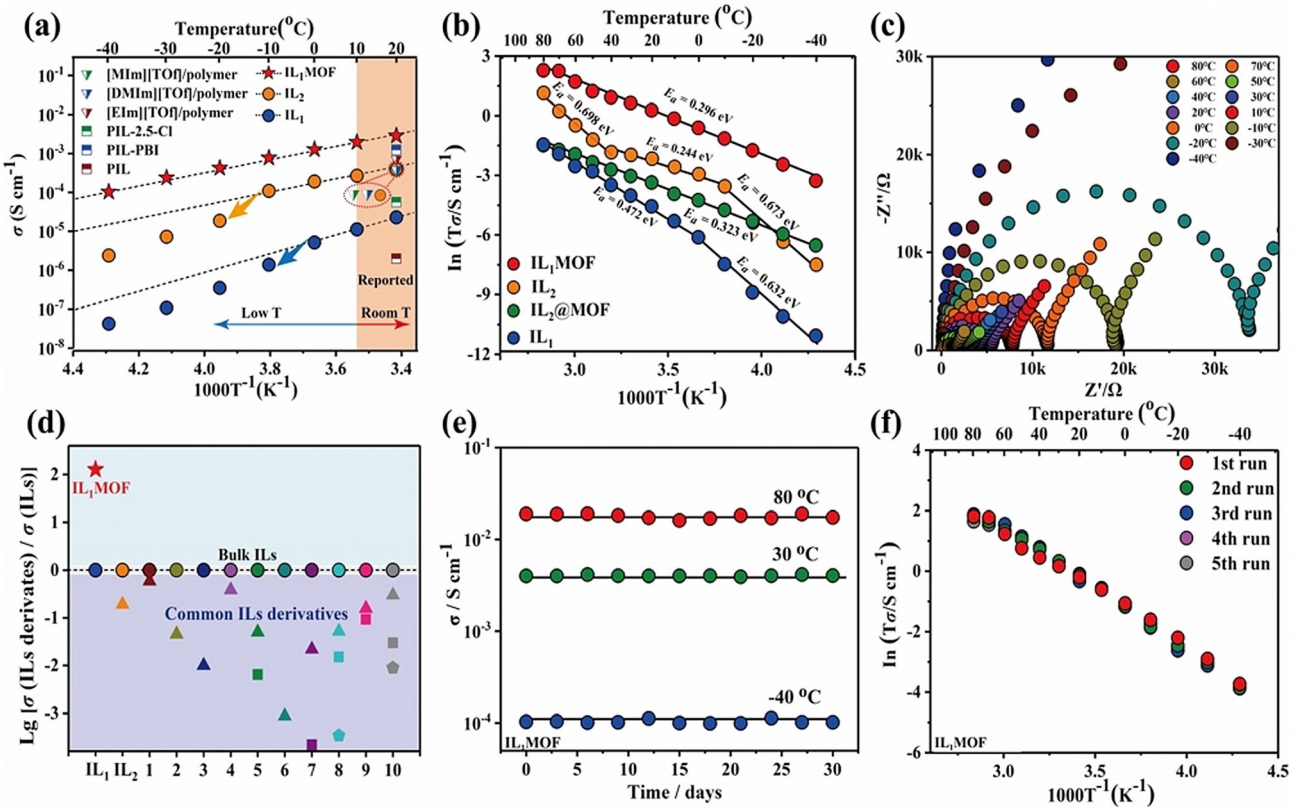

Figure 2. a) Several protic IL derivatives reported in room temperature region (10–20 °C, anhydrous), and this work with temperature low to −40 °C (Table S5, Ref. [18a,b]). The arrows infer the abrupt deviations away from the dashed lines to guide the eye. (b) Temperature-dependent conductivities of **IL_1MOF**, **IL_2@MOF**, **IL_1**, **IL_2** (Table S5). c) Nyquist plots of **IL_1MOF** from −40 to 80 °C. d) Survey of reported bulk ILs (balls), their derivatives and this work (●**IL_1**,★**IL_1MOF**, ●**IL_2**, ▲**IL_2@MOF**) around room temperature. Derivatives with same parent IL are shown as the same color and aligned at the same horizontal coordinate (1–10). The ordinate axis is the $\lg\sigma_{(ILs\ derivative)}/\sigma_{ILs}$ for clarity. Dashed line along the bulk ILs (balls) indicates a conductivity limitation of normal IL derivatives (see Table S6 and Ref. [15, 19a–c, 11b]). e) Long-term stabilities and f) recycle tests of **IL_1MOF** at different temperature.

and pre-heated at 60 °C under vacuum overnight before measurements. It is found that both **MIMS-MOF** and MSA show negligible conductivities even at 150 °C (10^{-8}–10^{-9} S cm^{-1}, Figure S10 and S11), likely due to a lack of dissociated H^+ to act as a mobile charge carrier. The conductivity of MSA at 150 °C is 2.11×10^{-8} S cm^{-1}, and decreased to 9.01×10^{-10} S cm^{-1} at 110 °C. Protic ILs usually have high conductivities at temperature above 100 °C, but at room temperature or below their conductivities dramatically decrease[18,20] (Figure 2a). This drop in conductivity is because the intermolecular interactions are strongly enhanced as lowering temperature, which decreases the ionic mobility of ILs.[20] This inherent drawback seriously limits ILs use as electrolyte at subzero temperatures, such as in on-board automotive application in cold climates or at high-altitude.[20b] Notably, **IL_1MOF** possesses distinct properties and shows a conductivity of 1.03×10^{-4} S cm^{-1} at −40 °C, no abrupt conduction dropping was found. This value is 4 orders of magnitude higher than that of its parent **IL_1** in bulk (Figure 2a, b, S12, S13 and Table S5).

When the temperature is increased from −40 to 80 °C, **IL_1MOF** shows enhanced conductivity with linear Arrhenius behavior (Figure 2a and b). At 20 °C, the conductivity of **IL_1MOF** reaches to 2.87×10^{-3} S cm^{-1}, a value 2 orders of magnitude higher than that of **IL_1**. This value is also 1–3 orders magnitude higher than those of the reported solid protic IL derivatives such as ionogels[18a] and poly(ionic liquid)s,[18b] and 2 times higher than that of commercial Nafion-115 (1.25×10^{-3} S cm^{-1}) with 98% relative humidity at similar temperature.[19d] Although, when temperature is increased from −40 to 80 °C, the conductivity of **IL_1** sharply increases by 5 orders of magnitude. At 80 °C, the conductivity of **IL_1MOF** is 1.89×10^{-2} S cm^{-1}, which is still 2 orders of magnitude higher than that of **IL_1**. Meanwhile, from −40 to 80 °C, **IL_1MOF** also has 1–2 orders of magnitude higher conductivity than **IL_2**. Until now, the surveyed solid IL derivatives were all reported with lower conductivities than their counterpart bulk ILs at room temperature (Figure 2d and Table S6), and this phenomenon becomes more pronounced when increasing temperature.[5,6,11,15] Interestingly, the conductivity of **IL_1MOF** is unexpectedly higher than these of **IL_1** and **IL_2** in the whole measured temperature range (Figure 2a and b). Meanwhile, **IL_1MOF** also exhibits the highest conductivities from 30 to 80 °C when compared to other MOF-based anhydrous proton conductors (see Table S7 and Figure S14).

IL_1MOF shows good long-term stability with almost unvaried conductivity at −40, 30 or 80 °C for 30 days,

respectively. This stability is also supported by PXRD patterns, with unchanged patterns from −40 to 80 °C (Figure 2e, f, and S6). Retention tests by soaking **IL_1MOF** and **IL_2@MOF** in deionized water for 20 minutes were conducted and compared (Table S3, Figure S15 and S16). Conductivity of **IL_2@MOF** decreased by 4 orders of magnitude after soaking. In contrast, **IL_1MOF** showed significantly less change before (1.89×10^{-2} S cm^{-1}) and after (5.30×10^{-3} S cm^{-1}) soaking (Figure S18). These results suggest **IL_1MOF** exhibits lower risk for leakage than ILs@support[6] as well as ILs@MOF.[11,14a,15]

Conductivities of **IL_1MOF** were compared with those of **IL_2@MOF** to help determine structure-property relationships (Figure 1 and Figure 2, Scheme S2). The measured conductivities of **IL_1MOF** are 1–2 orders of magnitude higher than that of **IL_2@MOF** (10^{-6}–10^{-3} S cm^{-1}) from −40 to 80 °C (Figure 2b). Since **IL_1MOF** has the same components to that of **IL_2@MOF** (ESI, Table S4), the conductivity difference between them should be attributed to their structural differences. PXRD measurements show that the peaks around 5–7 degree of **IL_2@MOF** remarkably vanished as compared with these of UiO-67 (Figure S6c). This phenomenon signifies the random state of ILs within **IL_2@MOF** that enhanced background diffraction as that commonly observed for other ILs@MOF,[11,14a,15] rather the collapsed framework. The recovered PXRD patterns of **IL_2@MOF** after soaking in methanol further confirms this point of view (Figure S6c). On the other hand, **IL_1MOF** shows almost intact peaks at low 2θ angle when compared with those of UiO-67 and **MIMS-MOF** (Figure 1c). This result suggests **IL_1** in **IL_1MOF** is in a long-range ordered arrangement.

To help elucidate more details from the structure, quantitative solid-state ^{13}C NMR (nuclear magnetic resonance) spectra techniques of dipolar dephasing magic-angle-spinning (DD MAS) for **IL_1MOF** at ambient temperature were recorded (Figure 3a, **S19** and **S20**). The peaks can be divided into two groups: 1) the peaks ranging from 170 to 120 ppm can be assigned to the carbons on the carboxylate groups, benzene and imidazolium rings; 2) the peaks ranging from 60 to 20 ppm can be attributed to the carbons on MSA and the methylene of MIMS side chain. Compared to the immobile backbone carbons of **IL_1MOF** in the first groups,[16a] the carbons in the latter group have sharper signals, indicating a "motional narrowing"[11a,15] arising from the MSA and -MIMS (Figure 1). The peaks at 39.79 and 36.33 ppm with a 3.77:1 integration ratio can be assigned to the carbon of MSA and the methylene directly connected to the sulfonate group of -MIMS, respectively. These two peaks have smallest line width than other peaks, suggesting more labile MSA and the terminal group of -MIMS with respect to that backbone in **IL_1MOF**. The ratio between MSA and H_2BPDC-MIMS plays important role in deciding the states of their complexes. As shown in Figure S22, when it is less than or equal to 1.89:1, the complex is a solid with an immobile component; when it is higher than 1.89:1, the complex is a viscous sticky liquid; when it equals 3.78:1, the **IL_1** is a fluid liquid with mobile

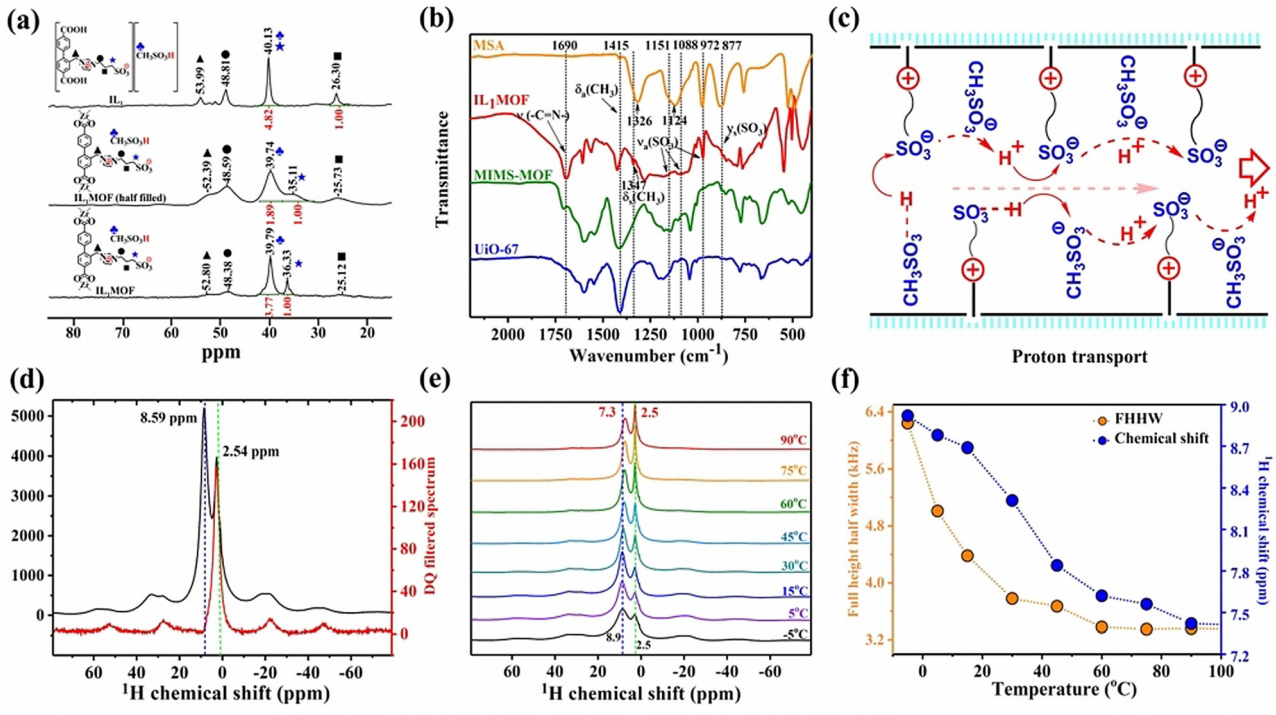

Figure 3. a) Solid-state ^{13}C NMR (DD MAS) of **IL_1** (at 7 kHz), **IL_1MOF** and half-filled **IL_1MOF** (at 15 kHz) at ambient temperature (also see Figure S19–S21). b) FT-IR spectra of UiO-67, **MIMS-MOF**, **IL_1MOF** and neat MSA. c) Diagram of the proton transport mechanism in **IL_1MOF**. d) ^{1}H MAS (black) and ^{1}H DQF (red) SSNMR spectra (at 10 kHz) of **IL_1MOF** at room temperature, and temperature-dependent ^{1}H SSNMR spectra e) with tetramethylsilane as reference and adamantane (^{1}H, $\delta = 1.85$ ppm) as a secondary reference.[24a] The DQ signals were excited and reversed by using the back-to-back sequence.[24b] f) Plots of chemical shifts and FHHW of the acid proton resonance of **IL_1MOF** as a function of temperature.

components, as confirmed by its ^{13}C (Figure 3a) and ^{1}H CP MAS (cross polarization magic-angle-spinning) (Figure S21–S25) SSNMR (solid-state ^{1}H nuclear magnetic resonance) spectra. The line width of the peaks of the labile carbons (39.79 and 36.33 ppm) of **IL_1MOF** are between those of liquid **IL_1** (merging at 40.13 ppm) and the proposed solid-state half-filled **IL_1MOF** (39.71 and 35.11 ppm) (Figure 3a, and S19–S21). Therefore, the ^{13}C NMR and above mentioned PXRD data suggest **IL_1** in **IL_1MOF** has its ILs part [-MIMS][MSA] resembling a structure of liquid crystal with the motion ability between solid and liquid state.[21] The different chemical environments of carbons in **IL_1**, **IL_1MOF** (half-filled), and **IL_1MOF** are further confirmed by their different chemical shifts (Figure 3a). Although the MSA and the terminal sulfonate group of -MIMS are labile as discussed above, electrostatic contact and H-bonding between the MSA and -MIMS locate the MSA in site in an ordered structure within **IL_1MOF**, well accounting for the sharply different PXRD patterns between **IL_1MOF** and **IL_2@MOF** (Figure 1c and S6).

Solid FT-IR spectra are shown and compared in Figure 3b and S7. Importantly, besides the characteristic stretching bands of the neat -SO_3^- ($\nu_a SO_3^-$ at 1151 cm^{-1} and $\nu_s SO_3^-$, 877 cm^{-1}) in **MIMS-MOF**, new strong $\nu_a SO_3^-$ bands toward lower wavenumbers at 1088 and 972 cm^{-1} are found in **IL_1MOF** with the weak $\nu_s SO_3^-$ (877 cm^{-1}) unchanged. The separation between two $\nu_a SO_3^-$ bands of 116 cm^{-1} in **IL_1MOF** is due to the (-SO_3^-) S=O···H (-SO_3H) interactions and the proton exchange within the [-MIMS][MSA] core region.[17] The significantly broadened bands from 1151 cm^{-1} ($\nu_a SO_3^-$) to 877 cm^{-1} ($\nu_s SO_3^-$) range of **IL_1MOF** with respect to that of **MIMS-MOF** and MSA further suggests that a hydrogen-bonding network is formed between -SO_3^- and -SO_3H. Thus, in the crystalline **IL_1MOF**, a long-range ordered hydrogen-bonding network forms, which may act to decrease the proton hopping activation energy (E_a).[14] This is demonstrated by the least-squares fits of the slopes of the temperature-dependent proton conductivities (Figure 2b). **IL_1MOF** show its E_a = 0.296 eV, which is lower than **IL_1** and **IL_2** (0.472 eV ≈ 0.698 eV), and **IL_2@MOF** (0.323 eV). The higher E_a values indicate the randomly arranged IL composites in **IL_1**, **IL_2** and **IL_2@MOF** have a vehicle mechanism for proton transport (Scheme 1). Comparatively, the long-range ordering arrangement of **IL_1** in crystalline **IL_1MOF** possesses a Grotthuss mechanism (Figure 3c), which facilitates facile proton transport.[22]

To investigate the origin of the high conductivity of **IL_1MOF** below room temperature, differential scanning calorimetry (DSC) of **IL_1**, **IL_2**, and **IL_1MOF** were performed. DSC profiles show endothermic peaks around −46.1 and −91.8 for the **IL_1** and **IL_2** during the up scan, respectively, signifying the vitrification processes (Figure S26). While, the exothermic DSC peaks observed for the ILs also infer that a phase transition occurs as temperature decreased, and thus the interactions among the components of ILs markedly increased with decreasing temperature. These events well account for the decreased conductivity for **IL_1** (onset at 0 °C) and **IL_2** (onset at −10 °C) as temperature is decreased (Figure 2a). Notably, there is no thermic event that occurs during the heating/cooling cycle within −150 to 80 °C range for **IL_1MOF** (Figure S26), indicating no phase transition. These results suggest the better dispersion of MSA within the MOF, and well account for that recyclable and stable conductivity of **IL_1MOF** at different temperatures (Figure 2d,e). Such results also indicate the ultramicropore regions (< 1 nm) inside the octahedron (containing 2.64 -MIMS, 10 MSA, cal. See ESI) and tetrahedrons (1.32 -MIMS, 5 MSA) of **IL_1MOF** have dispersed [-MIMS][MSA] well enough to suppress the formation of large ionic clusters and efficiently prevented a freezing at subzero temperature down to −150 °C. Therefore, the high conductivity of **IL_1MOF** at low temperature may be ascribed to the synergistic effect of its crystalline structure and confinement within ultramicropore channel. The former factor dictates and arranges **IL_1** in ordered arrays and allows for fast proton transport via (-SO_3^-) S=O···H (-SO_3H) network pathway[14] (Figure 3c), while the latter prevents ionic cluster from freezing[11] and thus leads to its high conductivity at −40 °C and linear Arrhenius behavior (Figure 2a,b) across a very wide temperature range.

To describe the proton dynamic and its correlation to the conductivity of **IL_1MOF**, solid-state ^{1}H nuclear magnetic resonance (SSNMR) spectroscopy was performed with double-resonance magic-angle-spinning (MAS) probe supporting rotors at 10 kHz. The room temperature SSNMR ^{1}H spectrum under one-plus excitation shows broad resonance signal with high intensity at 2.54 and 8.59 ppm (Figure 3d and e), which can be assigned to the -CH_3 proton and the acid proton of -SO_3H, respectively.[23] In a double-quantum filter (DQF) ^{1}H MAS NMR experiment, only the 2.54 ppm resonance is observable, further confirming its assignment to the MSA methyl group.[23b] Either long distance between proton-pairs or fast molecular motion on the NMR time scale may be attributed the absent DQ signal at 8.59 ppm due to weak dipole-dipole coupling between protons. For the large octahedral cage ($\varphi \approx 16$ Å) containing 2.64 -MIMS (≈ 7 Å across) and 10 MSA (≈ 2 Å across), the (-SO_3^-)H···(-SO_3H) is less than 4 Å of the detectable H-H couplings in DQ MAS experiment,[16b] which excludes the long distance between proton-pairs. So, the absent DQ signal 8.59 ppm should be ascribed to the fast acid proton motion. This point of view also is further confirmed by temperature-dependent ^{1}H NMR spectra from −5 to 90 °C of **IL_1MOF**. Significant and continuous ^{1}H chemical shifting to lower frequency (shift difference 1.6 ppm, Figure 3e) and gradually narrowing full height at half-width (FHHW) of the resonances of acid protons were observed as the temperature was increased (Figure 3f). The shifting together with that narrowing FHHW indicate the rapid proton exchange motions between -SO_3^- and -SO_3H and their contribution to the conductivity of **IL_1MOF**.[16b,23] In contrast, the unchanged ^{1}H chemical shift (2.5 ppm) (Figure 3e) with increasing temperature and that intact resonance of -CH_3 in the ^{1}H DQF spectra (Figure 3d) hint the $CH_3SO_3H/CH_3SO_3^-$ populate the equivalent sites owing to their immobility, with no contribution to the conductivity.[16,23a] These results demonstrate the conductivity of **IL_1MOF** is proton dominant conduction (Figure 3c).

Conclusion

The possibility of promoting an IL from an amorphous to a crystalline state was demonstrated for the first time by preparing **IL_1MOF** via a coordination self-assembly based reticular chemistry strategy. The **IL_1** ligand in **IL_1MOF** was arranged with long-range order but with a labile ionic center. This unique structure decreases the activation energy for proton transport and changes the proton conduction for **IL_1** from a vehicle mechanism to a Grotthuss mechanism, which facilitates fast proton transport to reach a state-of-the-art conductivity. As a result, **IL_1MOF** breaks though the inherent properties of its counterpart bulk ILs, including 1) a long-range ordered crystalline structure, enabling deeper insight into the structure-property relationship; 2) much higher conductivity by 2–4 orders of magnitude versus its highly conductive counterpart bulk IL across a wide temperature range, which have never been achieved by IL derivatives; 3) extending the working condition of IL past subzero temperatures by confining IL in ultramicropores and eliminating its phase transition down to −150 °C. This work provides a novel and feasible strategy to realize crystalline materials from an amorphous or even a liquid state, which may generate significant inspiration for designing a new-generation of IL materials with high performance for broader applications.

Acknowledgements

This work was supported by the NSF of China (22071157, 21371123, 21773245, 21822109, 21975254, 21905280, 2020000052), NSF of Beijing Municipality (No. 2172014) and Capacity Building for Sci-Tech Innovation-Fundamental Scientific Research Funds, the Key Research Program of Frontier Sciences, CAS (QYZDB-SSW-SLH023), the Strategic Priority Research Program of CAS (XDB20000000), International Partnership Program of CAS (121835KYSB201800), China Postdoctoral Science Foundation (2019M662254), and Youth Innovation Promotion Association CAS. We are grateful to Prof. Shuao Wang, Dr. Daxiang Gui of Soochow University, and Prof. Haijun Yang of Tsinghua University for SSNMR measurements. Great thanks also for discussion and help of Prof. Qiaowei Li, Bin-Bin Tu of Fudan University and Prof. Weixiong Zhang of Sun Yat-Sen University.

Conflict of interest

The authors declare no conflict of interest.

Keywords: electrolytes · ionic liquids · long-range order · metal–organic frameworks (MOFs) · proton conduction

[1] a) S. Karak, K. Dey, A. Torris, A. Halder, S. Bera, F. Hanheerampockil, R. Banerjee, *J. Am. Chem. Soc.* **2019**, *141*, 7572 – 7581; b) J. Tang, S. Namuangruk, W. Kong, N. Kungwan, J. Guo, C. Wang, *Angew. Chem. Int. Ed.* **2016**, *55*, 13979 – 13984; *Angew. Chem.* **2016**, *128*, 14185 – 14190; c) D. Wrapp, N. Wang, K. S. Corbett, J. A. Goldsmith, C.-L. Hsieh, O. Abiona, B. S. Graham, J. S. Mclellan, *Science* **2020**, *367*, 1260 – 1263; d) F. Yang, G. Xu, Y. Dou, B. Wang, H. Zhang, H. Wu, W. Zhou, J.-R. Li, B. Chen, *Nat. Energy* **2017**, *2*, 877 – 883.

[2] a) S. Knoppe, T. Burgi, *Acc. Chem. Res.* **2014**, *47*, 1318 – 1326; b) W.-J. Liu, L.-Z. Dong, R.-H. Li, Y.-J. Chen, S.-N. Sun, S.-L. Li, Y.-Q. Lan, *ACS Appl. Mater. Interfaces* **2019**, *11*, 7030 – 7036.

[3] a) G. K. H. Shimizu, J. M. Taylor, S. Kim, *Science* **2013**, *341*, 354 – 355; b) S. Bureekaew, S. Horike, M. Higuchi, M. Mizuno, T. Kawamura, D. Tanaka, N. Yanai, S. Kitagawa, *Nat. Mater.* **2009**, *8*, 831 – 836; c) H. Xu, S. Tao, D. Jiang, *Nat. Mater.* **2016**, *15*, 722 – 726; d) Y. Ye, L. Zhang, Q. Peng, G.-E. Wang, Y. Shen, Z. Li, L. Wang, X. Ma, Q.-H. Chen, Z. Zhang, S. Xiang, *J. Am. Chem. Soc.* **2015**, *137*, 913 – 918.

[4] a) A. S. Amarasekara, *Chem. Rev.* **2016**, *116*, 6133 – 6183; b) P. Wang, S. M. Zakeeruddin, P. Comte, I. Exnar, M. Grätzel, *J. Am. Chem. Soc.* **2003**, *125*, 1166 – 1167.

[5] a) R. Sasi, S. Sarojam, S. J. Devaki, *ACS Sustainable Chem. Eng.* **2016**, *4*, 3535 – 3543; b) P. Nellepalli, L. C. Tomé, K. Vijayakrishna, I. M. Marrucho, *Ind. Eng. Chem. Res.* **2019**, *58*, 2017 – 2026.

[6] a) J. Le Bideau, L. Viau, A. Vioux, *Chem. Soc. Rev.* **2011**, *40*, 907 – 925; b) B. Lin, S. Cheng, L. Qiu, F. Yan, S. Shang, J. Lu, *Chem. Mater.* **2010**, *22*, 1807 – 1813; c) P. C. Marr, A. C. Marr, *Green Chem.* **2016**, *18*, 105 – 128; d) B. Lin, W. Yuan, F. Xu, Q. Chen, H. Zhu, X. Li, N. Yuan, F. Chu, J. Ding, *Appl. Surf. Sci.* **2018**, *455*, 295 – 301; e) Md. A. B H. Susan, T. Kaneto, A. Noda, M. Watanabe, *J. Am. Chem. Soc.* **2005**, *127*, 4976 – 4983.

[7] T. L. Greaves, C. J. Drummond, *Chem. Rev.* **2015**, *115*, 11379 – 11448.

[8] S. R. Batten, N. R. Champness, X. M. Chen, J. Garcia-Martinez, S. Kitagawa, L. Öhrström, M. O'Keeffe, M. P. Suh, J. Reedijk, *Pure Appl. Chem.* **2013**, *85*, 1715 – 1724.

[9] a) A. Schoedel, M. Li, D. Li, M. O'Keeffe, O. M. Yaghi, *Chem. Rev.* **2016**, *116*, 12466 – 12535; b) H.-C. Zhou, S. Kitagawa, *Chem. Soc. Rev.* **2014**, *43*, 5415 – 5418; c) S. M. Cohen, *Chem. Rev.* **2012**, *112*, 970 – 1000; d) T. Zhang, W. Lin, *Chem. Soc. Rev.* **2014**, *43*, 5982 – 5993; e) Q. Yang, Q. Xu, H. L. Jiang, *Chem. Soc. Rev.* **2017**, *46*, 4774 – 4808; f) Y. Liu, A. J. Howarth, N. A. Vermeulen, S. Y. Moon, J. T. Hupp, O. K. Farha, *Coord. Chem. Rev.* **2017**, *346*, 101 – 111; g) H. Ji, K. Naveen, W. Lee, T. S. Kim, D. Kim, D.-H. Cho, *ACS Appl. Mater. Interfaces* **2020**, *12*, 24868 – 24876; h) W. J. Phang, H. Jo, W. R. Lee, J. H. Song, K. Yoo, B. Kim, C. S. Hong, *Angew. Chem. Int. Ed.* **2015**, *54*, 5142 – 5146; *Angew. Chem.* **2015**, *127*, 5231 – 5235; i) S. Mukhopadhyay, J. Debgupta, C. Singh, R. Sarkar, O. Basu, S. K. Das, *ACS Appl. Mater. Interfaces* **2019**, *11*, 13423 – 13432; j) B.-J. Yao, L.-G. Ding, F. Li, J.-T. Li, Q.-J. Fu, Y. Ban, A. Guo, Y.-B. Dong, *ACS Appl. Mater. Interfaces* **2017**, *9*, 38919 – 38930.

[10] a) F. G. Cirujano, *ChemCatChem* **2019**, *11*, 5671 – 5685; b) S. S. Nadar, L. Vaidya, V. K. Rathod, *Int. J. Biol. Macromol.* **2020**, *149*, 861 – 876; c) W. H. Chen, X. Yu, A. Cecconello, Y. S. Sohn, R. Nechushtai, I. Willner, *Chem. Sci.* **2017**, *8*, 5769 – 5780.

[11] a) K. Fujie, T. Yamada, R. Ikeda, H. Kitagawa, *Angew. Chem. Int. Ed.* **2014**, *53*, 11302 – 11305; *Angew. Chem.* **2014**, *126*, 11484 – 11487; b) Y. Yoshida, K. Fujie, D.-W. Lim, R. Ikeda, H. Kitagawa, *Angew. Chem. Int. Ed.* **2019**, *58*, 10909 – 10913; *Angew. Chem.* **2019**, *131*, 11025 – 11029.

[12] J. H. Cavka, S. Jakobsen, U. Olsbye, N. Guillou, C. Lamberti, S. Bordiga, K. P. Lillerud, *J. Am. Chem. Soc.* **2008**, *130*, 13850 – 13851.

[13] Y. H. Zhao, M. H. Abraham, A. M. Zissimos, *J. Org. Chem.* **2003**, *68*, 7368 – 7373.

[14] a) H. Chen, S. Y. Han, R. H. Liu, T. F. Chen, K. L. Bi, J. B. Liang, Y. H. Deng, C. Q. Wan, *J. Power Sources* **2018**, *376*, 168 – 176; b) M. Yoshizawa, H. Ohno, *Chem. Commun.* **2004**, 1828 – 1829.

[15] a) K. Fujie, K. Otsubo, R. Ikeda, T. Yamada, H. Kitagawa, *Chem. Sci.* **2015**, *6*, 4306 – 4310; b) K. Fujie, R. Ikeda, K. Otsubo, T. Yamada, H. Kitagawa, *Chem. Mater.* **2015**, *27*, 7355 – 7361.
[16] a) G. R. Goward, M. F. H. Schuster, D. Sebastiani, I. Schnell, H. W. Spiess, *J. Phys. Chem. B* **2002**, *106*, 9322 – 9334; b) Y. J. Lee, B. B. Bingöl, T. Murakhtina, D. Sebastiani, W. J. Meyer, G. Wegner, H. W. Spiess, *J. Phys. Chem. B* **2007**, *111*, 9711 – 9721.
[17] a) J. Kausteklis, V. Aleksa, M. A. Iramain, S. A. Brandán, *J. Mol. Struct.* **2019**, *1175*, 663 – 676; b) A. Martinelli, A. Matic, P. Jacobsso, L. Börjesson, A. Fernicola, S. Panero, B. Scrosati, *J. Phys. Chem. B* **2007**, *111*, 12462 – 12467.
[18] a) F. Yan, S. Yu, X. Zhang, L. Qiu, F. Chu, J. You, J. Lu, *Chem. Mater.* **2009**, *21*, 1480 – 1484; b) J. Lemus, A. Eguizábal, M. P. Pina, *Int. J. Hydrogen Energy* **2016**, *41*, 3981 – 3993; c) A. Fernicola, S. Panero, B. Scrosati, *J. Power Sources* **2008**, *178*, 591 – 595.
[19] a) M. Döbbelin, I. Azcune, M. Bedu, A. R. de Luzuriaga, A. Genua, V. Jovanovski, G. Cabañero, I. Odriozola, *Chem. Mater.* **2012**, *24*, 1583 – 1590; b) Q. Xu, X. Zhang, S. Zeng, L. Bai, S. Zhang, *ACS Sustainable Chem. Eng.* **2019**, *7*, 7892 – 7899; c) U.-H. Lee, T. Kudo, I. Honma, *Chem. Commun.* **2009**, 3068 – 3070; d) B. Wu, J. Pan, L. Ge, L. Wu, H. Wang, T. Xu, *Sci. Rep.* **2014**, *4*, 4334.
[20] a) O. Borodin, G. D. Smith, W. Henderson, *J. Phys. Chem. B* **2006**, *110*, 16879 – 16886; b) C. Wang, G. Zhang, S. Ge, T. Xu, Y. Ji, X. Yang, Y. Leng, *Nature* **2016**, *529*, 515 – 518; c) M. Yoshizawa, W. Xu, C. A. Angell, *J. Am. Chem. Soc.* **2003**, *125*, 15411 – 15419; d) J.-P. Belieres, C. A. Angell, *J. Phys. Chem. B* **2007**, *111*, 4926 – 4937; e) C. A. Angell, N. Byrne, J.-P. Belieres, *Acc. Chem. Res.* **2007**, *40*, 1228 – 1236.
[21] P. H. J. Kouwer, T. M. Swager, *J. Am. Chem. Soc.* **2007**, *129*, 14042 – 14052.
[22] K. D. Kreuer, *Chem. Mater.* **1996**, *8*, 610 – 641.
[23] a) G. Brunklaus, S. Schauff, D. Markova, M. Klapper, K. Müllen, H.-W. Spiss, *J. Phys. Chem. B* **2009**, *113*, 6674 – 6681; b) G. Ye, N. Janzen, G. R. Goward, *Macromolecules* **2006**, *39*, 3283 – 3290.
[24] a) C. R. Morcombe, K. W. Zilm, *J. Magn. Reson.* **2003**, *162*, 479 – 486; b) M. Feike, D. E. Demco, R. Graf, J. Gottwald, S. Hafner, H. W. Spiess, *J. Magn. Reson. Ser. A* **1996**, *122*, 214 – 221.

Manuscript received: August 6, 2020
Accepted manuscript online: September 30, 2020
Version of record online: November 13, 2020

